Fluid flow in a diametrally expanded CANDU fuel channel – Part 2: Computational study

M.H.A. Piro [a,b,*], M. Christon [c], B. Tensuda [b,d], M. Poschmann [a], M. Bruschewski [e,f], S. Grundmann [e], C. Tropea [g]

[a] Faculty of Energy Systems and Nuclear Sciences, Ontario Tech University, Oshawa, ON, Canada
[b] Fuel and Fuel Channel Safety Branch, Canadian Nuclear Laboratories, Chalk River, ON, Canada
[c] Computational Sciences International, Los Alamos, NM, USA
[d] University of Toronto Institute for Aerospace Studies, University of Toronto, Toronto, Canada
[e] Institute of Fluid Mechanics, University of Rostock, Rostock, Germany
[f] Institute of Gas Turbines and Aerospace Propulsion, Technische Universität Darmstadt, Darmstadt, Germany
[g] Institute of Fluid Mechanics and Aerodynamics, Technische Universität Darmstadt, Darmstadt, Germany

ARTICLE INFO

ABSTRACT

The current work presents investigations of flow through a 37-element CANDU nuclear fuel bundle residing within a deformed pressure tube. This scenario simulates the long-term effects of aging, whereby the pressure tube may experience up to 6% diametral creep, resulting in flow bypass and the concomitant increase in fuel temperature due to local undercooling. This work examines in high spatial detail the three-dimensional, three-component fluid velocity field through the fuel channel. A companion paper is dedicated to the experimental component of this work, which is based on Magnetic Resonance Velocimetry. In the present paper, computational fluid dynamic simulations have been performed with HYDRA using an implicit large eddy simulation to predict turbulent flow behavior. Together, an improved understanding has been gained in quantifying flow bypass, the evolution of geometry-induced inter-subchannel mixing, and various turbulent effects, such as recirculation, swirl, and separated flow. These capabilities are not possible with conventional experimental techniques or thermal-hydraulic codes. The overall goal of the combined works is to continue developing experimental and computational capabilities for future investigations to support nuclear reactor performance and safety.

1. Introduction

Unlike Light Water Reactors, CANDU power reactors have horizontally configured fuel channels that may experience appreciable diametral creep over the lifetime of the channel (i.e., up to ≈6% of diameter) (Piro et al., 2016a,b). This mechanism is due to large pressure differentials between the fuel channel and the calandria tube, high temperature, and the assistance of irradiation enhanced creep (Rodgers et al. 2016). The degree of diametral creep varies depending on the specific fuel channel and the specific reactor; however, the general trend observed is that higher power channels experience greater diametral creep and there tends to be a downstream-skewed cosine distribution that attains a maximum approximately two-thirds downstream from the inlet (DeAbreu et al. 2018).

As a consequence of diametral creep, the space on the top of the fuel channel increases and the coolant distribution, following the path of least resistance, flows more above the bundle in comparison to a normal non-deformed pressure tube. Hence, the coolant flow through the inner regions of the bundle is reduced, which in turn increases the local temperature field and ability to cool the bundle. Understanding internal flow conditions is therefore important in quantifying the cooling capability of individual fuel elements within the fuel bundle.

Established experimental methods are ineffective at accurately measuring fluid velocity within a fuel bundle due to physical obstructions or lack of optical access into the flow regime. Furthermore, while conventional thermal–hydraulic codes are effective at system level or bundle level analyses, they rely heavily on empirical correlations that are not universal in nature and are unable to capture local effects with high spatial fidelity.

This work examines the three-dimensional, three-component (3D3C) fluid velocity field in a model of a single fuel bundle with Magnetic Resonance Velocimetry (MRV) measurements and Computational Fluid Dynamics (CFD) using Large Eddy Simulations (LES). The overall aim of this combined study is to develop experimental

---

* Corresponding author at: Faculty of Energy Systems and Nuclear Sciences, Ontario Tech University, Oshawa, ON, Canada.
  E-mail address: markus.piro@uoit.ca (M.H.A. Piro)

and computational capabilities to provide high-resolution velocity data for nuclear reactor thermalhydraulic investigations that are currently not possible with conventional techniques. In brief, MRV can non-intrusively measure 3D3C velocity fields without requiring optical access to the measurement volume and without injection of tracer particles into the flow field.

The present paper is Part 2 of two companion studies. The overall aim of this combined study is to develop experimental and computational capabilities to provide high-resolution velocity data for nuclear reactor thermalhydraulic investigations. Part 1 in Bruschewski et al. (2019) focusses on the description of the experiments in a model of a CANDU fuel bundle within a 6% expanded pressure tube. The 3D3C mean velocity results obtained from MRV measurements are presented in detail. In the present paper (i.e., Part 2), CFD simulations were performed in the same fuel channel model to investigate detailed time-dependent turbulent behaviour of the flow through the same expanded pressure tube. The simulation results are compared to the experimental data in Part 1.

Due to the requirement of using non-ferromagnetic materials (i.e., polymers) in a Magnetic Resonance Imaging (MRI) scanner, the flow conditions that were analyzed – specifically temperature, pressure, and flow rate – were not the same as in-reactor conditions. Two other important differences from in-reactor conditions are that 1) only a single bundle was simulated rather than a string of 12 bundles, and 2) the pressure tube that was simulated was 6% larger in diameter than a conventional pressure tube. In a commercial reactor at end-of-life, the pressure tube will have experienced axial elongation, bowing, and diametral creep that varies across the length of the fuel channel. Recognizing these differences, which are extremely complex, the impetus of this work was to gain insight into the effects of flow bypass while further developing experimental and computational capabilities to provide high-resolution velocity data that cannot be produced by conventional techniques. The ultimate goal will be to extend this work in future work to more accurately capture the conditions relevant to nuclear safety analyses – principally, temperature, flow rates, materials, and geometry.

2. Background

This study describes the third experimental and computational campaign in investigating fluid flow through a CANDU fuel channel. The first investigation was a proof-of-concept that employed a simplified 8-element fuel bundle replica produced with polyamide material using a laser sintering process (Piro et al. 2016b). The second investigation used a 37-element bundle replica sitting in a pressure tube that was geometrically consistent with what is used in industry, specifically the Bruce Nuclear Generating Station (Piro et al. 2017).

The third investigation, which is described herein, examines flow through a 37-element bundle sitting on the bottom of a pressure tube that is 6% greater in diameter than a standard pressure tube. The intention is to maintain consistency with all other parameters in the previous investigations to isolate the differences of flow characteristics due to increased pressure tube diameter resulting in flow bypass. The replica bundle, fluid material, fluid flow rate, and measurement system were all consistent between the second and third campaigns – the only difference between the second and third campaigns was the pressure tube diameter.

Preliminary experimental (Bruschewski et al., 2016) and computational (Piro et al. 2016a) work on this third campaign were presented at the Organization for Economic and Cooperative Development Nuclear Energy Agency (OECD/NEA) & International Atomic Energy Agency (IAEA) Workshop on Computational Fluid Dynamics for Nuclear Reactor Safety at the Massachusetts Institute of Technology in 2016. In the preliminary work, some issues were observed with the computational mesh about insufficient quality and resolution in some regions of the domain. The mesh was recreated entirely to a higher standard, and a new LES computation was performed. The numerical results are presented in the companion paper (Piro et al., 2017). In the experimental part, which is presented herein, the analysis of the data was refined, and discussions on the significance of these results for nuclear reactor safety investigations were added.

A standard 37-element CANDU fuel bundle is shown on the left in Fig. 1 with salient features identified. In this design, fuel elements are mated together with Zircaloy-4 endplates to maintain spacing between adjacent fuel elements. Spacer pads are located in the mid-length of the bundle and prevent direct contact between elements. Bearing pads are appended to the outer ring of fuel elements to provide spacing from the adjacent pressure tube wall, as shown on the right in Fig. 1, which is intended to provide a pathway for water to travel for cooling purposes. The fuel bundle, pressure tube, and calandria tube collectively constitute the fuel channel.

Due to the horizontal configuration of fuel channels in the CANDU design, the fuel bundle sits on the bottom of the pressure tube. Over time, the pressure tube may experience diametral creep due to the large pressure differential between the inside and outside of the pressure tube (i.e., ≈10 MPa), which is accelerated by neutron fluence induced damage mechanisms. For the case of a diametrically crept pressure tube, the cross-sectional area of the top of the fuel channel increases and the coolant, following the path of least resistance, flows preferentially above the bundle (Bruschewski et al., 2016, Piro et al. 2016a). Hence, coolant bypasses the inner regions of the bundle, which in turn increases the local temperature field and affects the ability to cool the bundle. This phenomenon is commonly referred to as "flow bypass". Fig. 2 illustrates the difference between the cross-section of a bundle sitting in a normal and a diametrally crept pressure tube. The drawing on the right in Fig. 2 highlights the crescent-shape gap on the top of the fuel channel that gives rise to flow bypass.

All pressure tubes in operating CANDU reactors experience some diametral creep over sufficient periods of time (DeAbreu et al. 2018). The design end-of-life limit of pressure tube diametral creep
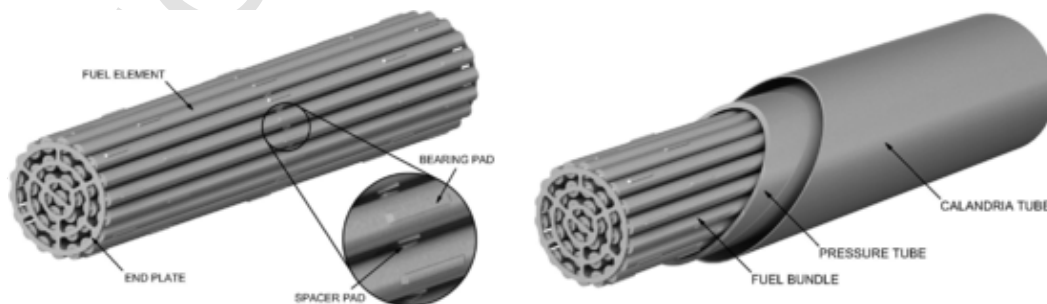

Fig. 1. A 37-element CANDU fuel bundle is shown on the left with salient features identified. The right image shows a 37-element CANDU fuel bundle sitting within a pressure tube, which is housed in a calandria tube (Piro et al. 2016b).
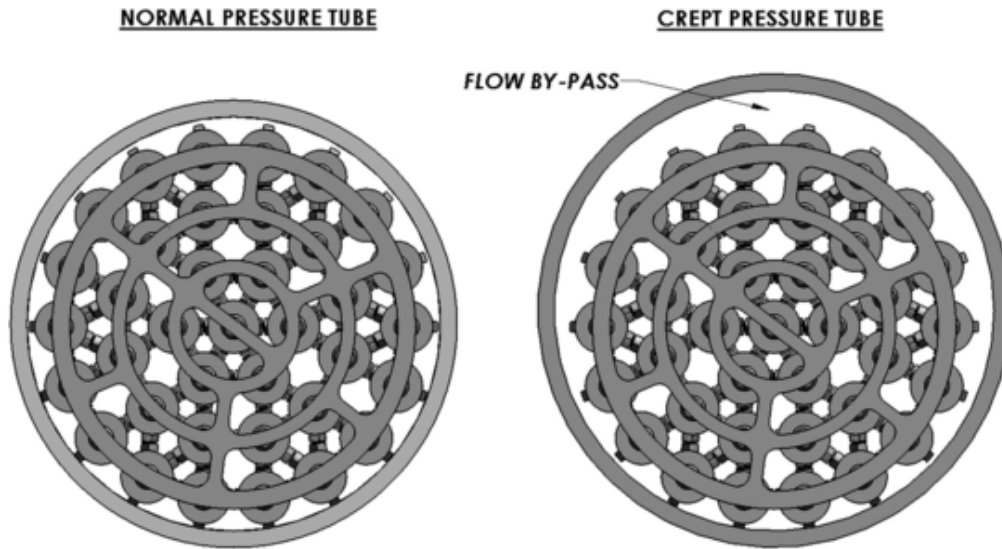
NORMAL PRESSURE TUBE   **CREPT PRESSURE TUBE**

FLOW BY-PASS

Fig. 2. An end view comparison of a 37-element CANDU fuel bundle sitting in a standard pressure tube (left) and a 6% crept pressure tube (right).

is 6% in some nuclear stations, and as long as sufficient bundle cooling can be demonstrated, higher diametral creep can be accepted as an end-of-life limit without the reactor being de-rated to satisfy safety concerns, which has a direct impact on performance. This limit is currently considered conservative (Holt 2008). Therefore, there is a direct financial incentive for industry to understand this phenomenon better to provide a technical basis for justifying a larger end-of-life limit for diametral creep.

Indeed, there are factors other than flow bypass that must be considered in regards to the long-term performance of pressure tubes, including changes to fracture toughness, tensile strength, and hydrogen pickup – all of which are affected by irradiation damage (Rodgers et al. 2016). In the overall performance of old pressure tubes, the present work serves two purposes:

- to quantify the effects of flow bypass to aid engineering safety analyses and fitness-for-service of CANDU fuel channels, and
- to further develop state-of-the-art experimental and computational fluid dynamic capabilities to support nuclear reactor performance and safety broadly.

3. Computational setup

The complex intricacies and orientations of the surfaces that bound the flow through the CANDU fuel bundle increase the convolution of fluid flow. For instance, the front and rear end plates induce separation and rotation, the skewed spacer pads induce swirl and the combination of various effects lead to inter-subchannel mixing. This is further complicated by the flow bypass region, whereby the fluid will follow the path of least resistance and bypass the fuel bundle, which changes with respect to the axial location. Therefore, the present simulations require sufficient spatial resolution to facilitate detailed comparison to the MRV measurements outlined in the previous section and described by Bruschewski et al. (2016).

Several previously published articles related to fluid flow through a CANDU fuel bundle have independently demonstrated that turbulence closure models based on the Reynolds Averaged Navier-Stokes (RANS) equations are reasonable for this particular flow problem, but generally do not perform as well as LES. These claims have also been supported by experimental measurements (Bhattacharya et al. 2012, Abbasian et al. 2009). Furthermore, RANS models un-

der-predict inter-subchannel mixing in a fuel bundle due to the inherent inability to capture turbulent anisotropy or quasi-periodic flow (for steady state cases) (Zaretsky 2014). For these reasons, LES equations were utilized to evaluate the time-dependent flow characteristics in the wall-bounded flow through a CANDU fuel bundle. The simulation was executed on the Graham High Performance Computing system, which is maintained by Compute Canada. A total of 256 cores were utilized with a total memory requirement of 296 GB.

3.1. Governing equations

The LES method presumes a threshold length and time scale below which the structure of the turbulent eddies can be universally modeled; thus, only eddies that exist in the larger scales need to be resolved. This is achieved by low-pass filtering of the time-dependent partial differential equations representing continuity and momentum under isothermal conditions. The continuity and momentum equations for incompressible isothermal fluid flow are respectively given as:

$$\frac{\partial \bar{u}_i}{\partial x_i} = 0 \tag{1}$$

$$\frac{\partial \rho \bar{u}_i}{\partial t} + \frac{\partial}{\partial x_j}\left(\rho \bar{u}_i \bar{u}_j\right) = -\frac{\partial \bar{p}}{\partial x_i} + \frac{\partial}{\partial x_j}\mu\left(\frac{\partial \bar{u}_i}{\partial x_j} + \frac{\partial \bar{u}_j}{\partial x_i}\right) - \frac{\partial \tau_{ij}}{\partial x_j} \tag{2}$$

In these equations, t is time, ρ is the fluid density, u_i is the i Cartesian component of velocity, x_i is the ith component of Cartesian spatial coordinate, p is the pressure, μ is the fluid viscosity, and τ_{ij} is the ij component of the residual stress tensor that comes about from filtering the Navier-Stokes equations. This stress tensor needs to be modeled to close the LES equations.

There are many variants of turbulence closure models that have been employed to filter and represent the subgrid-scale (SGS) terms in the LES equations. Implicit filtering of the governing equation is applied in this study. Instead of a fixed filter cut-off frequency normally used in explicit schemes, the present work employs an implicit approach with grid-adaptive variable filter sizes. In addition, rather than employing an SGS model, implicit modeling is applied in the

present study and hinges on the concept associated with the numerical regularization of the resolved-scale numerics due to the effects of SGS fluid dynamical effects (Grinstein et al. 2007). Here, the truncation error of the discretization and the associated dispersive characteristics combine to represent the physics of the unresolved scales unlike explicit LES models using SGS models. Specifically, with this method, a balance between phase speed and dissipation is constructed in a non-linear and monotonicity preserving procedure that respects the energy cascade throughout the discrete spectrum.

3.2. Solution method

The CFD code HYDRA was used in this work to solve the governing equations of conservation of mass and momentum. HYDRA is a subset of the Hydra Toolkit and it provides a general-purpose capability for simulating incompressible and low-Mach number flows. This software was successfully used in a previous study of flow in a 37-element CANDU fuel bundle with a non-deformed pressure tube that compared well to MRV measurements (Piro et al. 2016b). A virtually identical approach was applied to the present study. In fact, the same HYDRA input file was used in the third campaign with slight modifications to the mesh file, inlet boundary conditions, and post-processing options. This was done to ensure consistency between the two campaigns.

Numerical methods that "built-in" regularization, as is required for I-LES, may be found in stabilized finite element methods and some monotonicity-preserving finite volume methods. A detailed presentation of modified equation analysis and assessment of high-resolution (monotonicity-preserving) algorithms is described by Grinstein et al. (2007). A spectral analysis of the interplay between advective phase speed and dissipation for signals ranging from the integral to the grid Nyquist limit is described by Christon et al. (2004), Voth et al. (2004), and for HYDRA is discussed in Christon et al. (2016). The modified equation analysis is important in defining the form of implicit SGS terms. HYDRA also considers the spectral analysis that is critical in designing I-LES methods that accurately represent the grid-resolved eddies. The details of the non-linear, monotonicity-preserving advection scheme, and the associated phase speed and dissipation may be also found in the HYDRA Theory Manual (Christon, 2017).

In HYDRA, wall-functions are not used with an I-LES turbulence model, therefore requiring a mesh resolution down to a $y^+ \approx 1$ near walls. Here, the "+" superscript denotes normalization by wall variables, ν and $u_\tau = (\tau_w/\rho)^{0.5}$; where, ν and u_τ are the kinematic viscosity and friction velocity, respectively. In these definitions, τ_w is the shear stress at the wall. An automatic time-step controller is used with a fixed Courant-Friedrichs-Levy (CFL) condition in order to capture the eddy-turnover time scale associated with eddies in the regions between the rods in the bundle. Preliminary computations were carried out to assess the time-scale when a statistically stationary flow is established by monitoring the volume integrated kinetic energy for the flow domain. The volume integrated kinetic energy is converged after 2 s of physical simulation time, which indicated the starting point for the collection of turbulent statistics for the flow problem.

HYDRA is based on a hybrid projection algorithm for time-dependent, incompressible viscous flow (Christon et al. 2016). This hybrid finite element/finite-volume algorithm circumvents the usual divergence stability constraints – such as checkerboard modes in the pressure – and does not require explicit treatment of pressure modes using Rhie-Chow interpolation or a pressure-stabilized Petrov-Galerkin formulation. The hybrid projection algorithm relies on the so-called co-velocity approach, where dual-edge velocities that are centered at unique faces in the grid are made divergence-free and then used for advection. Together with a high-resolution advection scheme with a consistent edge-based treatment of viscous/diffusive terms, this yields a robust algorithm for incompressible flows.

Here, the second-order (in space and time) accurate projection method is used for the I-LES computations with a fixed-CFL automatic time-stepping algorithm. The construction of the high-resolution monotonicity-preserving algorithm with a second-order Trapezoidal rule in time permits an extended stability range. This permits stable, time-accurate I-LES computations with CFL values around 5–10. HYDRA relies on PETSc (Balay et al. 2015), the ML preconditioner from Trilinos (Heroux & Willenbring 2003), and Hypre (Falgout et al. 2015) for its linear solvers. In particular, Hypre's BoomerAMG is employed as a preconditioner to PETSc's CG solver for the pressure projection linear solve, while the momentum transport linear solve is performed using PETSc's FGMRES solver.

3.3. Computational geometry

For the sake of consistency, the geometry of the CANDU fuel bundle used in the CFD simulations was made using the same CAD model that was used to manufacture the polyamide bundle. This model is a correct geometric representation of a CANDU 37-element fuel bundle used in the Bruce Nuclear Generating Station. The computational geometry also included the pressure tube 50 mm upstream fluid region and 150 mm downstream fluid region. For a concentric non-deformed pressure tube, there would be a 0.89 mm gap between it and the bundle. In the present case, the pressure tube diameter is increased by 6% and the bundle rests on the bottom of the pressure tube, which is illustrated in Fig. 2.

3.4. Boundary conditions

In the physical experiment, a large diffuser adapts the flow supply system at the inlet of the test rig containing the fuel bundle with a nozzle at the outlet. Again, the pre-conditioning system used in the experiments (see Bruschewski et al. 2019) was designed to produce a flat velocity profile at the inlet of the test rig, which eliminates the need of including it in the computational geometry.

The operating fluid for this particular problem is incompressible light water at atmospheric pressure and at a temperature of 21 °C. At this state, the density of water is taken to be 997.2 kg•m^{-3} and the dynamic viscosity is 0.00089043 kg•m^{-1}•s^{-1} (Leung et al. 1999). The inlet was represented as a constant velocity inlet boundary condition with a value of 0.1052 m/s. Since the velocity profile of the experiment was flat (by design), it is appropriate to use a constant velocity for a boundary condition. Turbulent boundary conditions for turbulent kinetic energy and dissipation rate are not required at the inlet since the I-LES turbulence closure model was used. At the outflow boundary, a passive outflow condition was applied, which permits reverse flow while maintaining energy stability. Finally, all surfaces were treated as adiabatic solid walls with a no-slip, no-penetration boundary condition.

3.5. Mesh

Due to the lack of an explicit filter and explicit subgrid model in the I-LES formulations, the grid must be selected in a manner to ensure that the filtered length scales are small enough that the associated wavenumbers are well into the dissipative range of the turbulent spectrum. To this end, near-wall boundary elements need to be small and uniform in order to adequately resolve the flow behavior near the wall. However, for very complex flow geometries, the size

and uniformity of the cells along the wall are difficult to maintain during mesh generation.

In this study, the y^+ values were initially evaluated with preliminary calculations to verify that the no-slip, no-penetration boundary condition was sufficiently resolved. As the y^+ evolves both spatially and temporally, it was plotted periodically to verify that y^+ remained in a range suitable to resolve the wall boundary layers. The average calculated y^+ value over the fuel bundle and end-plate surfaces ranged from 1.5E to $2 \leq y^+ \leq 1.4$. The external pressure tube surface had a y^+ variation of $1.5E\text{-}3 \leq y^+ \leq 2.0$. The y^+ was based on the local wall shear and the first cell-center from the wall and was observed to be relatively smooth over all of the no-slip/no-penetration surfaces. We note in passing that the y^+ will vary both spatially and temporally, depending on the local flow structures that are present, e.g., in regions where there is strong swirling flow or separation. For this range of y^+ values, the laminar sublayer was resolved since the boundary layer region of the laminar sublayer extended to approximately $y^+ \sim 20$ (Chapman 1979). It is also noted that the majority of turbulent kinetic energy dissipation occurs in length scales of the order of $y^+ \approx 12$ to 30 (Tanahashi et al. 2004).

The geometry of the bundle was constructed with SOLIDWORKS (SolidWorks Corporation, 2015), which was then meshed with HEX-PRESS/HYBRID (NUMECA Inter. 2014). The geometry was meshed with 56.2 million cells, whereby 81% of the cells were hexahedrals, 15% were prisms, 2.4% were pyramids and 1.5% were tetrahedrals. HEX-PRESS/HYBRID was chosen for its ability to automatically generate high-quality hex-dominant meshes directly from CAD geometries, which proved to be very effective for such highly complex geometry.

Fig. 3 shows the computational mesh imposed on the fluid domain of the crept pressure and fuel bundle. In general, a five-layer inflation zone wa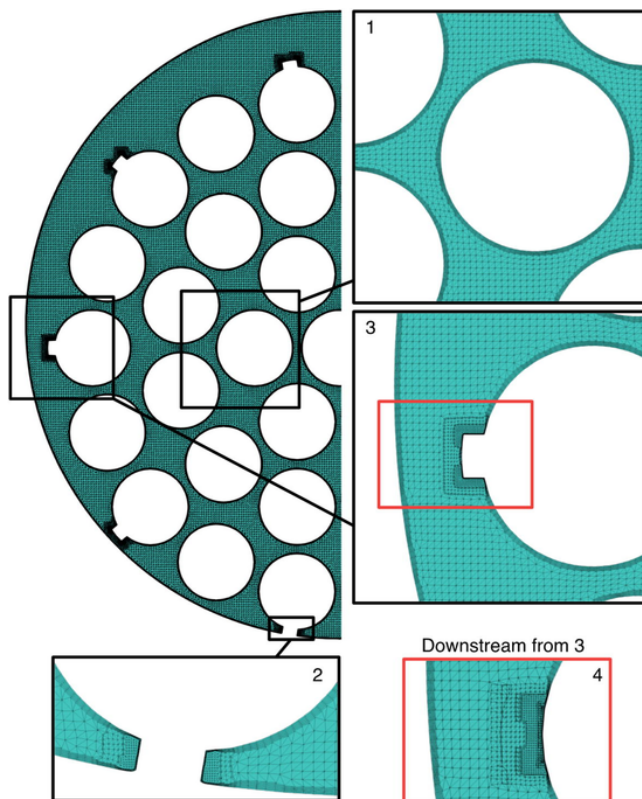s generated near the walls of the fuel elements to capture the boundary layer with overall high resolution within the subchannels. Inserts are shown to magnify the mesh near areas of interest. The insert labeled 1 illustrates the mesh in the fluid region between adjacent fuel elements in the bundle. A particular area of interest is the location where the bundle rests on the pressure tube on bearing pads. This is shown in the enlarged insert labeled 2 in Fig. 3 and indicates a good quality mesh. The inserts labeled 3 and 4 show the mesh at a bearing pad location and just downstream of this location. A fine resolution mesh is required downstream of the bearing pads to capture turbulent phenomena that could be induced by the presence of the bearing pad. Note that some of the mesh elements may appear distorted in this figure due to the projection of a three-dimensional mesh onto a two-dimensional plane.

The most challenging region of the domain to achieve a high-quality mesh is in-between adjacent spacer pads. This is due to the very narrow pathway coupled with the fact that spacer pads are askew from one another and mounted to fuel rods of opposing curvatures. Fig. 4 illustrates the mesh in this region. Note that despite the very narrow passageway, there are still 16 cells between the two solid surfaces and the vast majority of cells are hexagonal.

To reiterate, a completely new mesh was generated from the work of Piro et al. (2016a) which improved the mesh resolution and quality in key areas of the domain. Specifically, the mesh resolution was increased in the flow bypass region and additional cells were added to the inflation zone. To avoid dramatically increasing the total number of mesh cells while maintaining an appropriate mesh, the aspect ratio of the cells was increased in the axial direction from approximately 1.0 to 1.5. This was believed to be reasonable since the flow velocity is dominated in the axial direction, while still maintaining an aspect ratio that is generally known to be reasonable.

A mesh sensitivity analysis was not performed for this particular work for two reasons: 1) the mesh, geometry, and boundary conditions were all very similar to the work done for flow in a regular pressure tube (Piro et al., 2017), which did have a mesh sensitivity analysis, and 2) the computational requirements for this problem was so large and computing resources were so limited at the time the simulations were performed that it was not practical to perform additional simulations. This gives further reason to explore a rigorous turbulence model sensitivity analysis in future research.

3.6. Convergence criteria

In this study, the semi-implicit projection time-integration scheme (Christon, 2017) was used to understand the transient flow characteristic over the complex wall-bounded flow channel. The basic philosophy of the projection method is to provide a legitimate way to decouple the pressure and velocity fields, and establish an efficient computational method for transient incompressible flow simulations. Time integration was dynamically determined by HYDRA to constrain the maximum CFL number to 6.0 or a maximum time-step size of 10^{-4} s. The domain integrated kinetic energy, $\int \frac{\rho v^2}{2} d\Omega$, was computed by HYDRA with respect to time, which is also shown in Fig. 5. Here, Ω denotes the volume of the fluid domain.

Based on these calculations, in addition to evaluating the instantaneous velocity at pre-determined highly turbulent regions in the domain (see Fig. 6), a time of 2 s was selected as the starting point for calculating time-integrated statistics until the end of the simulation at 10 s. This time interval corresponded to approximately 100,000 time steps. The initial 2 s corresponds to approximately the region of flow transition; after then, the volume-integrated kinetic energy, and velocity/pressure time-histories indicate that the flow has reached a turbulent and statistically stationary state. Further-
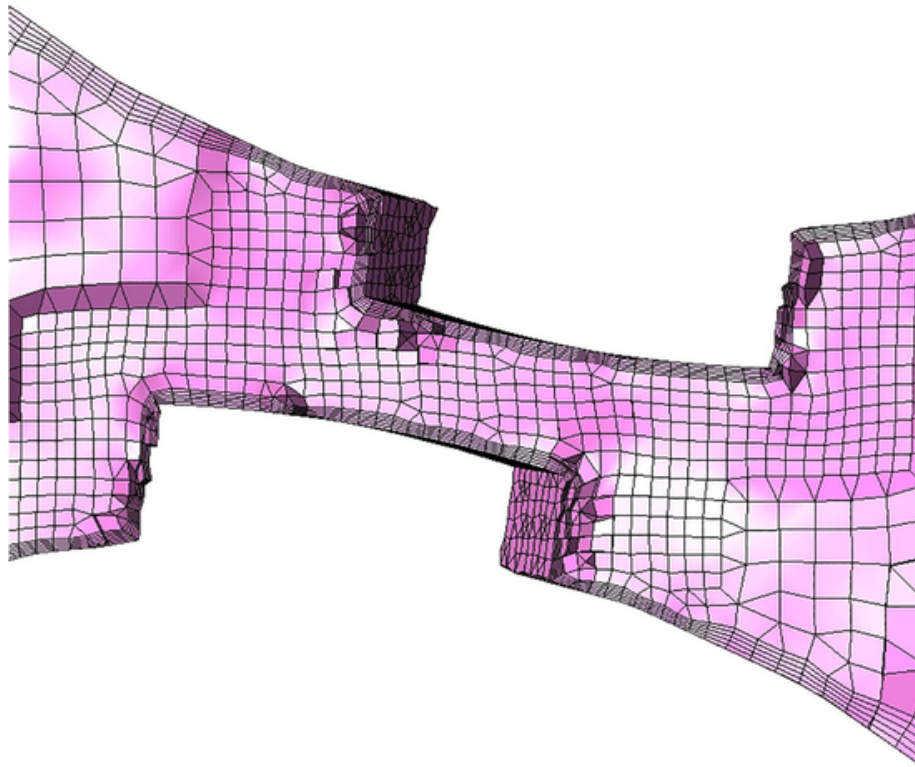

Fig. 3. The computational mesh representing the fluid region within the crept pressure tube is shown.

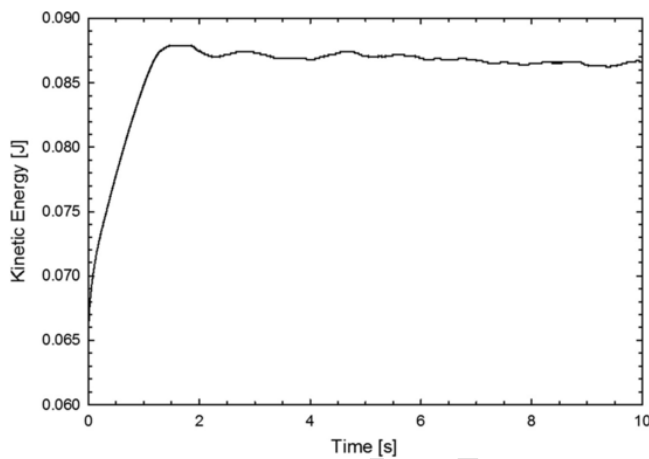**Fig. 4.** The mesh region between two adjacent spacer pads are shown.

Fig. 5. The computed volume-integrated kinetic energy and time step size is plotted with respect to simulation time.
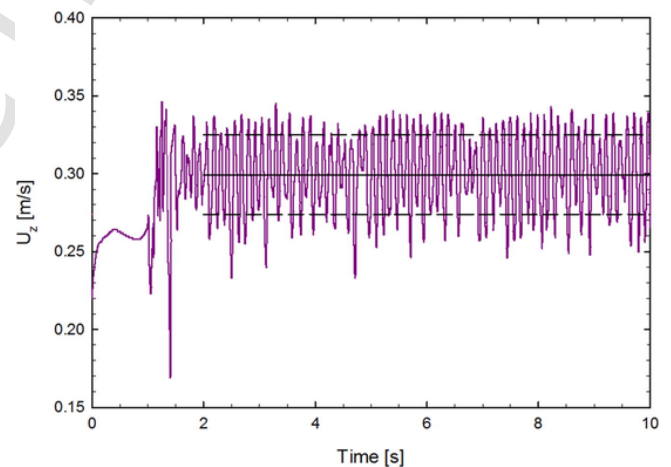

Fig. 6. The instantaneous axial velocity is plotted with respect to time in a highly turbulent region of the domain.

more, the flow velocity shown in Fig. 6 illustrates a clearly defined mean velocity and fluctuating component in the temporal range of 2–10 s. Convergence at the time step level was determined by ensuring that the normalized two-norm of the momentum residuals was $< 10^{-5}$, and the RMS norm of the divergence (continuity) was $< 10^{-7}$. In addition, the outlet flow rate was monitored to ensure that continuity of the CFD domain was satisfied as the simulation progressed.

4. Results

The space between neighboring fuel elements in a CANDU fuel bundle is termed a subchannel, through which the coolant is flowing to remove heat from the fuel elements. For good convective heat transfer, highly turbulent, thin boundary layers and high fluid velocity are advantageous. Inter-subchannel mixing improves the homog-

enization of coolant temperature within a CANDU fuel bundle under typical conditions, thus promoting the normalization of fuel element temperatures.

The lack of a wall-function and implicit modeling of the sub-grid scales for the I-LES method employed here means that a mesh that is too coarse would be overly dissipative. The adequacy of the computational assumptions used is qualified through comparison of the time-averaged axial velocity U_z obtained from the I-LES simulations with those of the MRV measurements.

Fig. 7 shows a contour plot of the time-averaged axial velocity magnitude across the midplane of the fuel channel, which gives an overall impression of how the fluid flow changes across the fuel bundle. At the inlet (left), the velocity profile is effectively constant. The flow accelerates as it enters the bundle due to the decreased free vol-
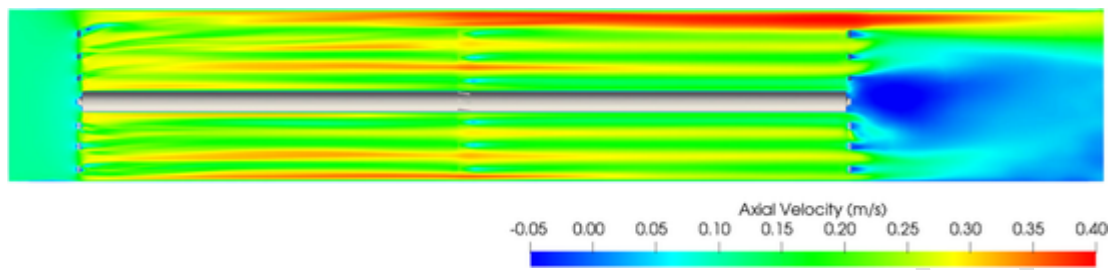
Fig. 7. A contour plot is shown of the time-averaged axial velocity midplane of the fuel channel. The increase in fluid velocity in the bypass region is quite evident. The fluid moves from left to right.

ume in the subchannels of the bundle. As the coolant progresses downstream, an increasing amount of fluid moves into the bypass region as it follows the path of least resistance, as indicated by the bright red regions on the top of the fuel channel. Note that the increased velocity in some inner parts of the bundle is relatively small regions in some of the subchannels that align with this plane. A wake is evident downstream of the bundle with the majority of the flow still following the bypass region.

Fig. 8 shows pathlines through the fuel channel coloured by the axial velocity. Sections of the fuel bundle were removed to more easily visualize internal subchannel flow. Similar to trends shown in Fig. 8, the velocity profile is fairly uniform at the inlet (left) and increases within the bundle where the free volume is obviously reduced. The pathlines illustrate some redistribution of flow upwards towards the bypass region, which ultimately has the highest velocity at the rear of the bundle. The pathlines shown in Fig. 8 demonstrate noticeable recirculation downstream from the bundle, which is likely contributed by both the rear end plate and the open volume. The effects of the rear end plate of one bundle on recirculation in the presence of an adjacent downstream bundle are not well understood.

The predicted vorticity is shown in Fig. 9 at 150 mm, which is approximately one-third of the length of the bundle and is a region where the flow is starting to noticeably redistribute to the bypass region (as seen, for example, in Fig. 9). The vorticity plot shown in Fig. 9 indicates maximum values near the walls, which is not surprising, but the more interesting regions stem from the outer fuel elements to the bypass region. These vortices are quite noticeable in this region and are indicative of appreciable rotation.

4.1. Comparison of simulation predictions to experimental results

Next, the mean flow field is compared to the MRV data described in the companion paper (Bruschewski et al. 2019). The distribution of U_z is considered at different axial positions shown in Fig. 10 through the contour plots in Fig. 11. In sequential order: just downstream from the bundle leading edge (Z = 10 mm); downstream from the first set of bearing pads (Z = 50 mm); at a flow region with aligned bearing pads (Z = 250 mm); at a region of the flow with the least flow obstructions (Z = 350 mm); at a flow region with staggered

bearing pads (Z = 400 mm); and at the outflow from the bundle (Z = 494 mm). In Fig. 11, the velocity is normalized by the time- and spatially-averaged inlet velocity to account for small differences in the flowrates at the inflow of the simulation and experiment.

At the axial location 10 mm downstream from the leading edge of the fuel bundle, the CFD and MRV trends compare very well qualitatively. However, the simulation predicts a higher degree of reversed flow induced by larger-scale turbulence eddies created as the relatively uniform bulk fluid begins to navigate through the bundle. It is possible that with this increase in turbulent kinetic energy immediately downstream from the leading edge may be accompanied by an increase in computational error due to false diffusion and/or inadequately capturing small turbulent structures. This deviation is expected as it is noted that just downstream of the bundle's leading edge, where the flow undergoes a high degree of acceleration, there is an inherently larger error in the MRV acquisition method (Bruschewski et al. 2019).

At 50 mm downstream of the bundle's leading edge, the contours of the simulations and experiments compare favorably. At this stage of flow development, the flow is being redistributed away from the bundle and towards the larger crevice at the top of the channel due to the crept pressure tube. As the contours at 250 mm to 400 mm indicate, much of this upward redistribution of the flow has occurred (more so in the MRV data) and a large percentage of the flow bypasses the bundle. The contours at the location of the downstream end plate are comparable, with similar degrees of reverse flow in both the measurement and simulation. The favourable comparison between the MRV and CFD data validate the numerical approach taken and confirm that the grid is sufficient to use I-LES without explicit wall functions.

The primary differences between measured and predicted axial velocities in Fig. 11 are in slightly over-predicted values in some of the subchannels, which is more noticeable in the second half of the bundle. However, as will be demonstrated in Fig. 12, the predicted values are within the experimental error and show a consistent trend.

Quantitative comparisons between predicted and measured axial velocities are shown in Fig. 12 at various axial locations (i.e., Z-direction) along both horizontal (i.e., X) and vertical (i.e., Y) coordinates. The coordinate system that is used in Fig. 12 is illustrated in
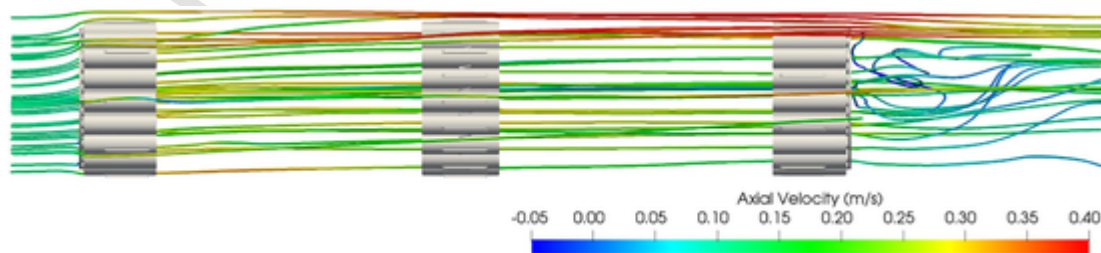

Fig. 8. Time-averaged streamlines colored by axial velocity are shown through the crept fuel channel, which illustrates the evolving flow bypass effect in addition to recirculation downstream from the bundle. Fluid flows from left to right.
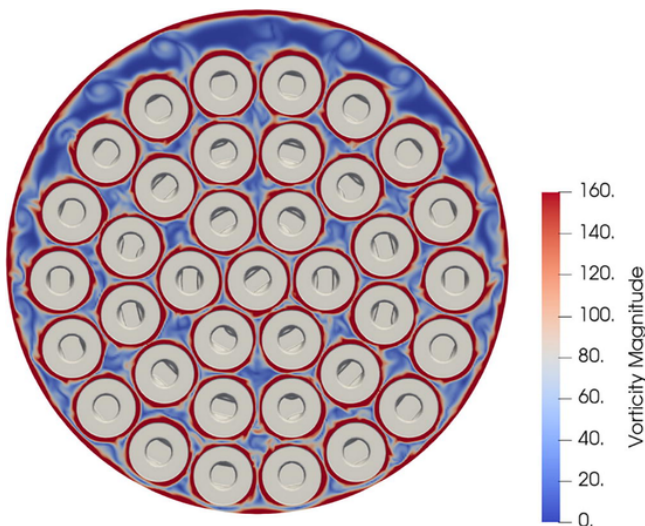
Fig. 9. A contour plot of the instantaneous vorticity magnitude is shown at $Z = 150$ mm, which illustrates the redistribution of fluid to the bypass region.
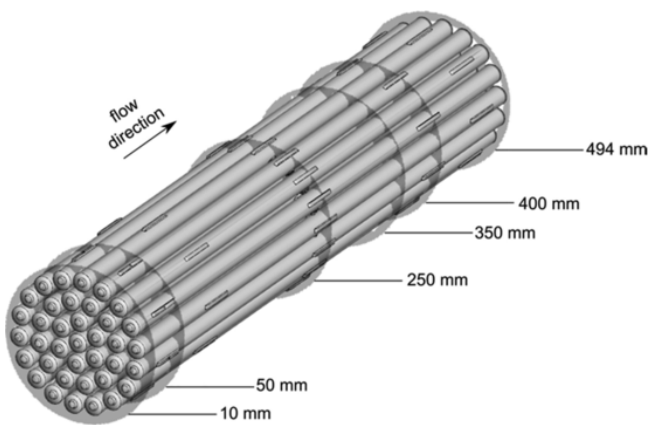

Fig. 10. Virtual planes are superimposed on a 37-element fuel bundle, which indicate the locations of contour plots that compare MRV measurements (Bruschewski et al. 2019) and CFD simulations in Fig. 11.

Fig. 13. Comparisons are made at 10 mm, 50 mm, 250 mm, and 400 mm locations downstream from the leading edge of the bundle in the Z-direction. Fig. 10 provides a useful point of reference for axial positions. Discontinuities in velocity data in Fig. 12 correspond to solid fuel elements in the bundle, which are also illustrated in Fig. 13.

There is generally good agreement between measured and predicted axial velocities in Fig. 12. General trends measured experimentally are well captured by CFD predictions, in addition to absolute values within experimental error. Near the front of the fuel bundle at $Z = 10$ mm, there is a known recirculation zone (Piro et al. 2017) following the upstream end plate, which affects the flow downstream. This generally appears to be well captured with the exception of two subchannel regions in the vertical direction around $Y = -12$ mm and $Y = 35$ mm. These differences are attributed to experimental error in insufficient voxel resolution.

At $Z = 10$ mm, one may note a sharp drop in axial velocity near $Y = 50$ mm. This is attributed to the effects of the highly turbulent region immediately downstream from the upstream endplate. This is not observed in the other plots in Fig. 12 because there aren't any other regions in these XY plots that correspond to the upstream endplate. Fig. 11, however, gives a more complete qualitative represen-

tation, which does indeed show a consistent drop in axial velocity at $Z = 10$ mm in regions that correspond to the upstream endplate.

Further downstream at $Z = 50$ mm, there is still generally good agreement with exception of a few subchannels, most notably in the vertical direction. Trends are fairly well captured further downstream at the bundle midplane (i.e., $Z = 250$ mm) with exception of some stagnation zones suggested by the MRV measurements. Intuitively, there is no physical reason why this would occur. Previous experience with MRV measurements of subchannel bundle flow by Piro et al (2016b) suggested that this is likely due to a relatively larger experimental error associated with insufficient voxel resolution in this region. Again, at this axial position, the cross-sectional area is reduced due to the presence of bearing and spacer pads (see Fig. 10). In the second half of the bundle at 400 mm, there is good agreement between predicted and measured velocities in both directions.

When viewing the axial velocity data in Fig. 12, one may notice that the peak velocities are not significantly greater in the bypass region in comparison to the lower parts of the fuel channel. This appears to be in contradiction to the general trend of flow redistribution to the bypass region that has been discussed throughout this manuscript; however, one should note that these plots are not a complete representation of flow through the bundle and should be understood with the trends shown in Fig. 11. For instance, Fig. 11 illustrates that the flow is still developing in the first half of the bundle with peak values in some subchannels being comparable to the bypass region. Furthermore, the peak values only represent a small geometric region of the subchannels. Therefore, the values shown in Fig. 12 are mainly intended to provide a quantitative comparison of predicted and measured values. A quantitative comparison of flow redistribution to the bypass region is shown in Fig. 14.

Fig. 14 illustrates the relative amount of fluid traveling through the bypass region with respect to the entire fuel channel as measured by MRV and predicted by CFD. These plots were calculated by taking a virtual cylinder with a diameter corresponding to the inner diameter of an as-received pressure tube (i.e., 103.4 mm). The detailed calculation of the error interval is provided in the companion paper (Bruschewski et al. 2019). This is visualized in Fig. 15.

It is important to note that the calculated flow bypass values from the MRV data in Fig. 14 have an inherent error and uncertainty associated with them (Bruschewski et al. 2019). First, the measured MRV quantities are based on calculating volumetric flow from the voxels assuming a constant volume, which is affected by partial volume errors at solid/liquid interfaces and distortion in the outer regions of the FOV. Also, there is some error when interpolating MRV data on the periphery of this virtual cylinder. The resolution is limited by voxel size (i.e., 0.78 mm), whereby the calculated values are very sensitive to the dimensions of the cylinder and any minor error can be quite noticeable. The CFD values have a much lower post-processing calculation error and uncertainty, due to the much high resolution of the mesh; therefore, the errors associated with CFD values are not dependent on post-processing, but rather with the manner that the physical problem has been simulated. For the aforementioned reasons, the MRV data in Fig. 14 have upper and lower bounds corresponding to the estimated error/uncertainty.

The comparison in Fig. 14 data between measured and predicted flow bypass quantities demonstrate consistent trends. The predicted values are consistently greater than measured quantities, and, interestingly enough, it appears somewhat constant at 2–3% higher than the average measured quantities. The sharp changes in MRV data correspond to the five fields of view, as described in section 2. Nevertheless, the trends agree with one another and the discrepancy appears to be consistent, which is likely due to the sensitivity of the
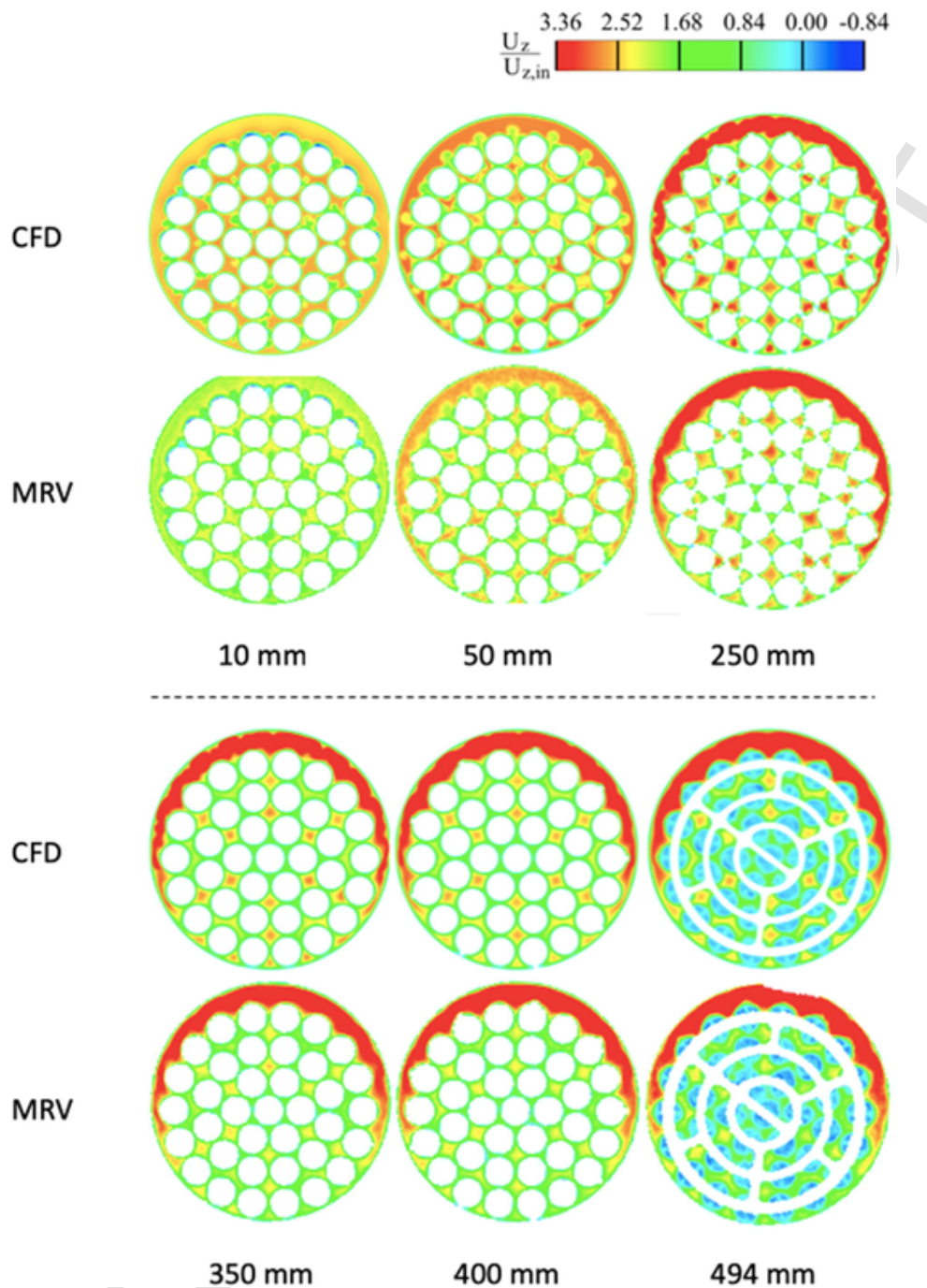
Fig. 11. Contour plots compare computed (CFD) axial mean velocities to measured (MRV) values from Bruschewski et al. (2019) at various axial positions.

calculation. Most importantly, the two data-sets are within the bounds of error/uncertainty.

Another meaningful comparison between measured and predicted values in the bypass region is shown in Fig. 16, which plots the average velocity in the bypass region relative to the average velocity in the bundle region. As to be expected, the average velocity increases downstream as a relatively greater portion of fluid travels through the upper region of the fuel channel. Three spikes are observed in the experimental data near Z = 0 mm, 250 mm, and 495 mm, which correspond to the upstream end plate, middle appendages, and downstream end plate, respectively. These spikes likely result from experimental errors, including partial volume effects, spatial encod-

ing, and velocity encoding errors. The discussion of these errors is provided in Bruschewski et al. (2019).

An important observation in Figs. 14 and 16 is that the relative volumetric flow rate and the average fluid velocity values somewhat stabilize near the end of the bundle. Since a fuel channel in a commercial reactor has 12–13 consecutive bundles, this observation implies that the flow is more or less fully developed by the end of the first bundle and the bypassing effect does not worsen. Nevertheless, these measurements demonstrate that ≈35% of the fluid bypasses the fuel bundle in a pressure tube that has experienced 6% diametral creep under the specific conditions examined herein.
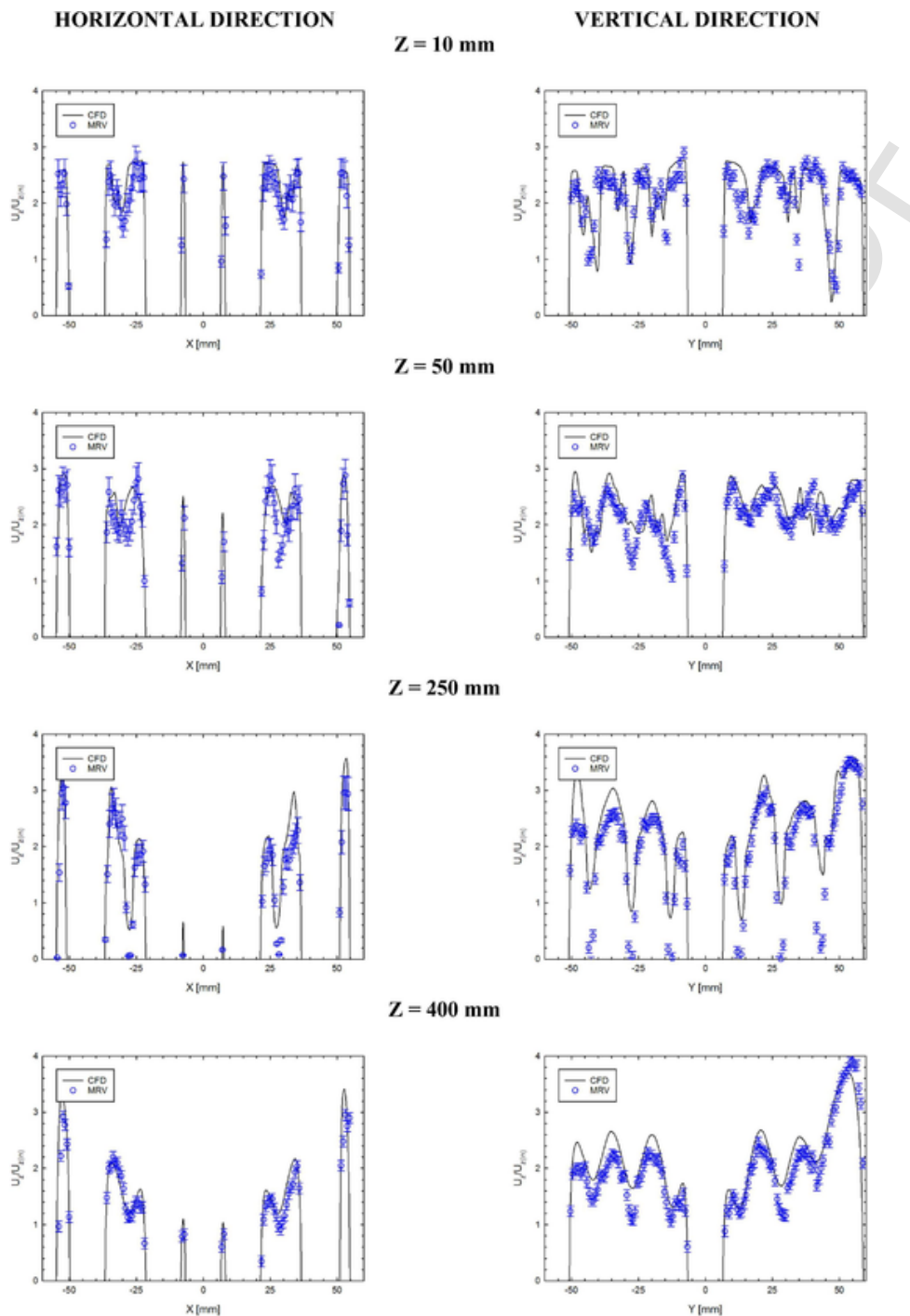
HORIZONTAL DIRECTION **VERTICAL DIRECTION**

Z = 10 mm

Z = 50 mm

Z = 250 mm

Z = 400 mm

Fig. 12. Comparison of the computed axial mean velocity with the experimental data in Bruschewski et al. (2019). The data is evaluated in horizontal (X) and vertical (Y) directions at various axial positions (Z).

5. Discussion

Again, the investigations described in this work were not precise representations of in-reactor conditions. Differences include fluid temperature, fluid hydrostatic pressure, fluid volumetric flow rate, fluid material, structural materials, a non-uniform heat source (or lack thereof), number of fuel bundles, and the geometry of a deformed pressure tube. One of the most important parameters that differs in this analysis compared to what is experienced in-reactor is Re – these analyses applied a Re that is much less than what is experienced in-reactor. Future research should investigate flow conditions that are more representative of in-reactor conditions. Having the ability to quantify the distribution of fluid flow through a fuel bundle sitting in a crept pressure tube is important to understand the cooling capability of a fuel bundle. These analyses provide important data to support the degree of reactor de-rating, which may otherwise be overly conservative.

As shown in Fig. 14, about 35% of the coolant bypasses the fuel bundle by the end of the 6% expanded fuel channel; similarly, in Fig. 16, the average fluid velocity in the bypass region is about dou-
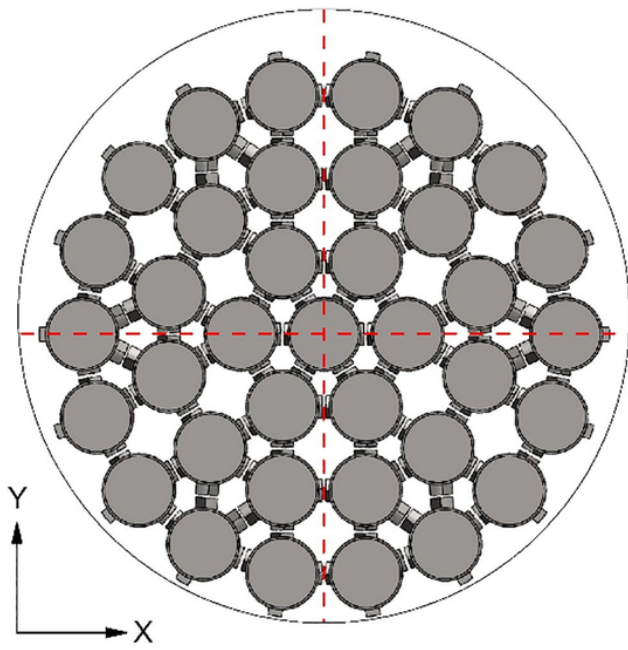
Fig. 13. A cross-sectional view of the diametrally crept fuel channel is shown. The X and Y co-ordinates identified in this figure correspond to the velocity data shown in Fig. 12.
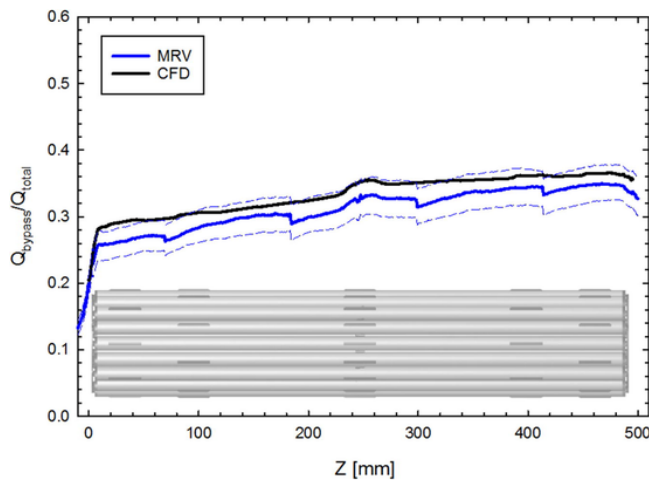

Fig. 14. A comparison between predicted and measured values of the fraction of flow that bypasses the bundle. The dashed lines represent the upper and lower error bands of MRV measurements.

ble the average value in the bundle. These results indicate that a relatively large fraction of the coolant bypasses the bundle, which affects fuel temperatures and the ability to cool the bundle.

Another discrepancy that is worth noting is that a single fuel bundle was used in this campaign whereas a 12-bundle string is used in a commercial reactor. One could expect that the effect of the marked increase in turbulence near the leading edge of the first bundle is diminished in a 12-bundle string. It is unclear how the axially varying diameter of the pressure tube effects flow through the bypass region across entire fuel channel. Similarly, there are uncertainties as to how the bundle azimuthal position affects flow, which may differ between adjacent bundles. Moreover, the turbulent features observed downstream from a bundle in this work would be complicated if there was an adjacent bundle downstream. Needless to say, there are many areas to further explore in future investigations.
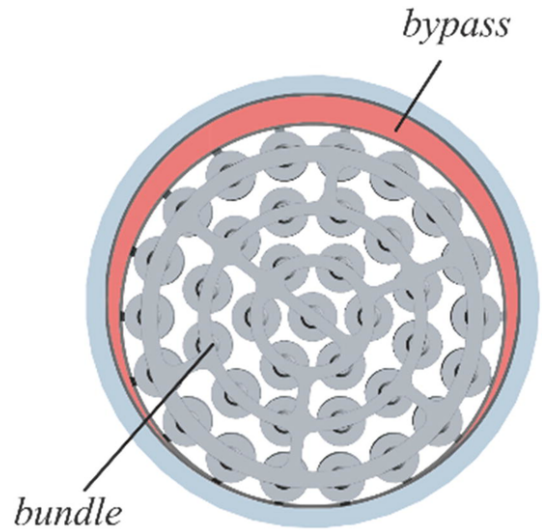

Fig. 15. The bypass and bundle regions are identified with respect to the comparisons shown in Figs. 14 and 16.
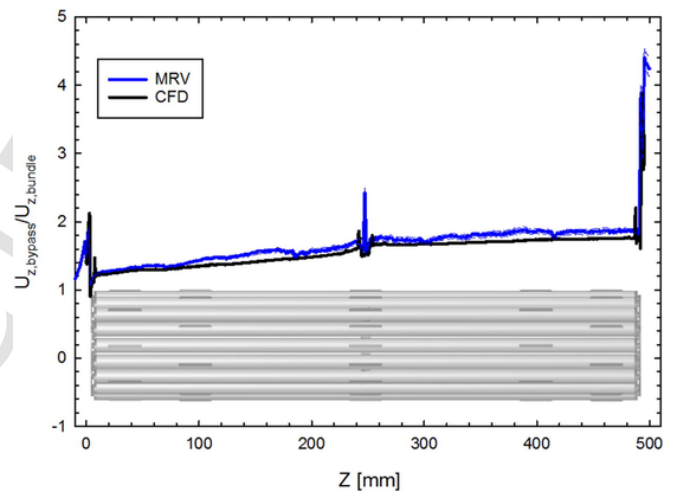

Fig. 16. A comparison of predicted and measured ratios of the average axial velocity in the bypass region relative to the bundle region.

The computational requirements to execute the simulations in this work was extremely high and required large high-performance computing resources. Considering that the simulation executed in this work was at a much lower Re than what is experienced in-reactor, one would require an even higher resolution mesh to investigate realistic flow conditions, which would considerably increase the computational requirements. This is simply impractical for industrial purposes. It would be prudent for future investigations to include a concerted turbulence model sensitivity analysis to assess the performance of many different turbulence models for CANDU fuel channel CFD simulations to objectively inform engineering analyses.

Progress has been made in advancing MRV as an emerging technology, which has demonstrated capabilities of value to the nuclear industry. There are no other experimental techniques currently available that can fully capture the velocity field within a fuel bundle. Furthermore, these measurements have given confidence in the numerical simulation approach. Future research could move towards more realistic in-reactor conditions, most notably achieving a more comparable Re, to help guide safety analyses in industry. Indeed, one must be cognizant of differences between the conditions that have been investigated herein in comparison to in-reactor conditions;

however, what's important here is that the quantity of flow that by-passes the bundle can now be measured and provide the mechanism to objectively informing engineering safety assessments to the industry.

6. Conclusions

Computational and experimental analyses have been presented of three-dimensional, three-component velocity distributions of light water flowing through a 37-element CANDU fuel bundle model sitting in a 6% diametrally expanded pressure tube replica at isothermal conditions. The impetus of this work was to better understand and quantify the effects of flow bypass, whereby coolant water preferentially bypasses the fuel bundle. MRV measurements and CFD predictions demonstrated that up to ≈35% of the fluid bypasses the bundle under these conditions (i.e., single bundle, uniformly expanded fuel channel, isothermal fluid). Also, it has been demonstrated that the average fluid velocity in the by-pass region is about twice that of the fluid in the bundle region. Generally speaking, CFD simulations agreed well with MRV measurements, which validates the approach and gives credence to applying this simulation framework to future investigations. While the temperature, pressure, and flow rate of the fluid investigated in this work are not fully representative of in-reactor conditions, significant progress has been made in developing experimental and computational capabilities to investigate fluid flow through a CANDU fuel channel in high spatial detail to support nuclear reactor safety assessments.

Uncited references

Dominguez-Ontiveros et al. (2012), Leung (2004), Moin and Mahesh (1998), Rao et al. (2014).

Acknowledgements

References

Abbasian, F., Yu, S.D., Cao, J., 2009. Experimental and Numerical Investigations of Three-Dimensional Turbulent Flow of Water Surrounding a CANDU Simulation Fuel Bundle Structure Inside a Channel. Nucl. Eng. Des. 239, 2224–2235.

Balay, S., Abhyankar, S., Adams, M., Brown, J., Brune, P., Buschelman, K., Dalcin, L., Eijkhout, V., Gropp, W., Karpeyev, D., Kaushik, D., Knepley, M., Curfman McInnes, L., Rupp, K., Smith, B., Zampini, S., Zhang, H., 2015. "PETSc User Manual", Argonne National Laboratory, Technical Report ANL-95/11 Rev 3.6.

Bhattacharya, A., Yu, S.D., Kawall, G., 2012. Numerical Simulation of Turbulent Flow Through a 37 Element CANDU Fuel Bundle. Ann. Nucl. Energy 40, 87–105.

Bruschewski, M., Freudenhammer, D., Piro, M.H.A., Tropea, C., Grundmann, S., 2016. New Insights Into The Flow Inside CANDU Fuel Bundles Using Magnetic Resonance Velocimetry. Proc. Comp. Fluid Dyn. Nucl. React. Safety, Cambridge, USA.

Bruschewski, M., Piro, M.H.A., Tropea, C., Grundmann, S., 2019. Fluid flow in a diametrally crept CANDU fuel channel – part 1: experimental study. Nucl. Eng. Des. in review (Note to editor/typesetter: this is a companion paper that was submitted with this article; please update reference accordingly).

Chapman, D.R., 1979. Computational Aerodynamics Development and Outlook. AIAA Journal 17, 1283–1313.

Christon, M.A., Martinez, M.J., Voth, T.E., 2004. Generalized Fourier Analysis of the Advection-Diffusion Equation – Part I: One-Dimensional Domains. Inter. J. Num. Meth. Fluids 45, 839–887.

Christon, M.A., Bakosi, J., Nadiga, B.T., Berndt, M., Francois, M.M., Stagg, A.K., Xia, Y., Luo, H., 2016. A Hybrid Incremental Projection Method for Thermal-Hydraulics Applications. J. Comp. Phys., accepted.

Christon, M.A., 2017. "The Hydra Toolkit Computational Fluid Dynamics Theory Manual", CSI-2015-1. Rev. A Computational Sciences International.

DeAbreu, R.F., Bickel, G.A., Buyers, A.W., Donohue, S.A., Dunn, K., Griffiths, M., Walters, L., 2018. Temperature and neutron flux dependence of in-reactor creep for cold-worked Zr-2.5Nb, Zirconium in the Nuclear Industry: 18th Inter. Symp., Ed: R.J. Comstock, A.T. Motta. ASTM International 938–964.

Dominguez-Ontiveros, E.E., Hassan, Y.A., Conner, M.E., Karoutas, Z., 2012. Experimental benchmark data for PWR rod bundle with spacer-grids. Nucl. Eng. Des. 253, 396–405.

R. Falgout, A. Cleary, J. Jones, E. Chow, V. Henson, C. Baldwin, P. Brown, P. Vassilevski, U. Meier Yang, 2015. "Hypre User's Manual", Lawrence Livermore National Laboratory.

Grinstein, F.F., Margolin, L.G., Rider, W., 2007. Implicit Large Eddy Simulation: Computing Turbulent Fluid Dynamics. Cambridge University Press.

Heroux, M.A., Willenbring, J.M., 2003. "Trilinos Users Guide", Sandia National Laboratories, Technical Report SAND2003-295

Holt, R.A., 2008. In-reactor deformation of cold-worked Zr-2.5Nb pressure tubes. J. Nucl. Mater. 372, 182–214.

Leung, L., 2004. "Experimental Studies on Critical Heat Flux in Support of the Advanced Fuel Design", 8th International Symposium on Heat Transfer. Beijing, China.

L.K.H. Leung, K.F. Rudzinski, B. Verma, D.C. Groeneveld and A. Vasic, "Thermalhydraulics Evaluation Package (TEP V3.0) – A User-friendly Software Package for Evaluating Thermalhydraulics Parameters in Tubes and Bundles", Proceedings of the 9th International Topical Meeting on Nuclear Reactor Thermalhydraulics (NURETH), San Francisco, USA (1999)

Moin, P., Mahesh, L., 1998. Direct numerical simulation: a tool in turbulence research. Annu. Rev. Fluid Mech. 30, 539–578.

Piro, M.H.A., Wassermann, F., Bruschewski, M., Freudenhammer, D., Grundmann, S., Kim, S.J., Christon, M., Berndt, M., Azih, C., Tropea, C., 2016. Experimental and computational investigation of flow bypass in a 37-element CANDU fuel bundle in a crept pressure tube. Proc. Comp. Fluid Dyn. Nucl. React, Safety, Cambridge, USA.

Piro, M.H.A., Wassermann, F., Grundmann, S., Leitch, B.W., Tropea, C., 2016. Progress in on-going experimental and computational investigations within a CANDU fuel channel. Nucl. Eng. Des. 299, 184–200.

Piro, M.H.A., Wassermann, F., Grundmann, S., Tensuda, B., Kim, S.J., Christon, M., Berndt, M., Nishimura, M., Tropea, C., 2017. Fluid flow investigations within a 37 element CANDU fuel bundle supported by magnetic resonance velocimetry and computational fluid dynamics. Inter. J. Heat Fluid Flow 66, 27–42.

Rao, Y.F., Cheng, Z., Waddington, G.M., 2014. Assessment of ASSERT-PV for prediction of critical heat flux in CANDU bundles. Nucl. Eng. Des. 276, 216–227.

Rodgers, D., Griffiths, M., Bickel, G., Buyers, A., Coleman, C., Nordin, H., St Lawrence, S., 2016. Performance in pressure tubes in CANDU reactors. CNL Nucl. Rev. 5 (1), 1–15.

Tanahashi, M., Kang, M., Miyamoto, S.J., T., 2004. Shiokawa and T, Miyauchi, "Scaling law of the fine scale eddies in turbulent channel flows up to Reτ = 800". Inter. J. Heat Fluid Flow 25, 331–340.

Voth, T.E., Martinez, M.J., Christon, M.A., 2004. Generalized Fourier Analysis of the Advection-Diffusion Equation – Part II: Two-Dimensional Domains. Inter. J. Num. Meth. Fluids 45, 889–920.

Zaretsky, A., 2014. Simulation of Intersubchannel Mixing in a Triangular Nuclear Fuel Bundle Geometry. Thesis, McMaster University, Hamilton, ON, Canada, MSc.

SolidWorks Corporation, 2015. SolidWorks User's Guide.

Numeca Inter., HEXPRESS/Hybrid User Manual, Version 11 (2014)